



Impact of 2-hydroxypropyl- β -cyclodextrin inclusion complex formation on dopamine receptor-ligand interaction – A case study

Lukas Zell^{a,c}, Thomas S. Hofer^d, Mario Schubert^{e,f}, Alexander Popoff^{a,c}, Anna Höll^{a,c}, Moritz Marschhofer^{a,c}, Petra Huber-Cantonati^{b,c}, Veronika Temml^{a,c}, Daniela Schuster^{a,c,*}

^a Department of Pharmaceutical and Medicinal Chemistry, Institute of Pharmacy, Paracelsus Medical University, 5020 Salzburg, Austria

^b Department of Pharmaceutical Biology, Institute of Pharmacy, Paracelsus Medical University, 5020 Salzburg, Austria

^c Research and Innovation Center for Novel Therapies and Regenerative Medicine, Austria

^d Institute of General, Inorganic and Theoretical Chemistry, Center for Biochemistry and Biomedicine, University of Innsbruck, 6020 Innsbruck, Austria

^e Department of Biosciences and Medical Biology, University of Salzburg, 5020 Salzburg, Austria

^f Department of Chemistry, Freie Universität Berlin, 14195 Berlin, Germany

ARTICLE INFO

Keywords:

2-hydroxypropyl- β -cyclodextrin

Inclusion complex

Dopamine receptor ligands

In silico

In vitro

Semi-empirical quantum chemistry

ABSTRACT

The octanol–water distribution coefficient ($\log P$), used as a measure of lipophilicity, plays a major role in the drug design and discovery processes. While average $\log P$ values remain unchanged in approved oral drugs since 1983, current medicinal chemistry trends towards increasingly lipophilic compounds that require adapted analytical workflows and drug delivery systems. Solubility enhancers like cyclodextrins (CDs), especially 2-hydroxypropyl- β -CD (2-HP- β -CD), have been studied in vitro and in vivo investigating their ADMET (adsorption, distribution, metabolism, excretion and toxicity)-related properties. However, data is scarce regarding the applicability of CD inclusion complexes (ICs) in vitro compared to pure compounds. In this study, dopamine receptor (DR) ligands were used as a case study, utilizing a combined in silico/in vitro workflow. Media-dependent solubility and IC stoichiometry were investigated using HPLC. NMR was used to observe IC formation-caused chemical shift deviations while in silico approaches utilizing basin hopping global minimization were used to propose putative IC binding modes. A cell-based in vitro homogeneous time-resolved fluorescence (HTRF) assay was used to quantify ligand binding affinity at the DR subtype 2 (D_2R). While all ligands showed increased solubility using 2-HP- β -CD, they differed regarding IC stoichiometry and receptor binding affinity. This case study shows that IC-formation was ligand-dependent and sometimes altering in vitro binding. Therefore, IC complex formation can't be recommended as a general means of improving compound solubility for in vitro studies as they may alter ligand binding.

1. Introduction

The octanol–water distribution coefficient ($\log P$) has been a major factor in the drug design and development processes since the introduction of quantitative structure–activity relationship approaches (QSAR) [1]. Lipophilicity was pioneered by Hansch and colleagues and also featured in Lipinskis 'Rule of Five' (Ro5) concept, limiting $c\log P$ to

<5. Amongst other parameters such as molecular weight (M_w) and hydrogen bond acceptors and –donors (HBA and HBD), lipophilicity plays a crucial role in describing properties of (orally) bioavailable compounds and their pharmacokinetic ADME (absorption, distribution, metabolism and excretion) characteristics [2,3]. Comparative assessments of successful oral drugs and compounds in development showed that violations of the $\log P$ limit are associated with undesirable effects

Abbreviations: AA, ascorbic acid; ADME, adsorption, distribution, metabolism and excretion; CD, cyclodextrin; COSMO, conductor-like screening model; CNS, central nervous system; CTB, CellTiter blue; DR, dopamine receptor; DR subtype 2, D_2R ; FDA, Food and Drug Administration; GPCR, G-protein coupled receptor; GRAS, generally regarded as safe; HB, hydrogen bond; HBA, hydrogen bond acceptor; HBD, hydrogen bond donor; 2-HP- β -CD, 2-hydroxypropyl- β -CD; HTRF, homogeneous time-resolved fluorescence; IC, inclusion complex; inc., incubation; LOD, limit of detection; $\log P$, water–octanol distribution coefficient; LOQ, limit of quantification; MP, mobile phase; M_w , molecular weight; PSB, phase solubility study; Ro5, Rule of Five; SCC DFTB, self-consistent charge density functional tight binding; SD, standard deviation; SN, supernatant; TFA, trifluoroacetic acid; w/o, without.

* Corresponding author.

E-mail address: daniela.schuster@pmu.ac.at (D. Schuster).

<https://doi.org/10.1016/j.bcp.2024.116340>

Received 8 February 2024; Received in revised form 10 May 2024; Accepted 4 June 2024

Available online 5 June 2024

0006-2952/© 2024 The Authors. Published by Elsevier Inc. This is an open access article under the CC BY license (<http://creativecommons.org/licenses/by/4.0/>).

such as poor aqueous solubility, increased unspecific protein binding, increased metabolic turnover and accumulation in tissues [4]. From a pharmacodynamics point of view, increased lipophilicity might be associated with promiscuous ligand-receptor interactions in vitro as well as toxicity in vivo [5]. This is also reflected in a study by Leeson and Springthorpe that showed that lipophilicity has remained relatively unchanged in approved oral drugs since 1983 [6]. In contrast, other Ro5 parameters like molecular mass as well as O plus N and OH plus NH atom counts (corresponding to HBAs and HBDs) are currently increasing. Interestingly, the same study showed that drug discovery projects in medicinal chemistry produce research compounds with higher molecular mass and lipophilicity compared to approved oral drugs (both historical and recent) and compounds in clinical development. Those statistics, starting in 1990, highlight increased median logP values of 4.1 and M_w of 450 Da, whereas oral drugs were characterized by values of 3.1 and 432, respectively. Another study by Gleeson et al highlighted a similar trend regarding research compounds included in the ChEMBL database [7]. Their data showed that roughly 25 % of highly potent compounds (binding affinities ≤ 1 nM) possessed a logP > 5. While this divergence between successfully approved drugs and current research compounds is surprising, it can be explained by the changing landscape of target proteins, also reflected in the drug development portfolios of major pharmaceutical companies. While G-protein coupled receptors (GPCRs) represent a highly druggable target (20 % of all drugs approved since 1983), the ‘golden age of GPCR structural biology’ starting in the early 2000s further drove the elucidation of their three-dimensional (3D) structures [8]. Consequently, specific binding sites were elucidated for many GPCRs, revealing important lipophilic sites crucial for ligand binding and (in-)activation [9]. More than 90 % of non-sensory GPCRs are expressed in the brain, thus, targeting them involves crossing the blood-brain barrier to render drugs or drug candidates active in the central nervous system (CNS) [10]. In general, CNS-targeting drugs (and compounds in development) are characterized by logP values of up to 5.8 with the majority residing in between logP 4 and 5 [11,12]. Therefore, the increasing interest in researching compounds with higher logP values highlight the need for optimized and adapted in vitro assays.

While ligand-protein affinity is often the key determinant for biological activity, it can't always be measured directly. Especially GPCR-targeted studies are oftentimes bound to cell-based assays, since structural integrity of the transmembrane receptors is dependent on intact and functional cell membranes [13]. Traditionally, radioligand binding (RLB) assays were the gold standard in determining binding affinities in vitro, however, due to high costs and radioactive waste, alternative methods were needed [14]. Homogenous time-resolved fluorescence (HTRF) assays constitute one such method that allows for determining binding affinities for a variety of GPCRs without the use of radioactive material in a semi-high throughput approach [15,16]. HTRF-based binding affinity assays, like cell-based in vitro assays in general, suffer from compound solubility issues (especially in higher logP ranges) due to the aqueous composition of the assay buffers in use [17]. While logP and solubility are limiting factors in in vitro studies, those limitations are not necessarily directly transferrable to in vivo settings, where bioavailability and oral systemic exposure are influenced by a multitude of different factors [18].

The use of typical solvents like ethanol or DMSO has been shown to be cytotoxic in cell-based setups also in low concentrations such as ≥ 1 % and ≥ 0.5 %, respectively [17]. To prevent solvent-induced cytotoxic phenomena, cyclodextrins (CDs) have been of major interest due to their capability of improving compound solubility and stability without interfering with cellular integrity [19]. The CD subtypes α , β and γ differ in their numbers of glucopyranose monomeric units, M_w , size and volume of their cavities as well as aqueous solubility [20,21]. While especially β -CD shows a particularly low aqueous solubility, replacement of the 2-OH with a 2-hydroxypropyl (2-HP) moiety (resulting in 2-HP- β -CD) increases solubility over 80-fold [22]. Moreover, 2-HP- β -CD

provides improved physicochemical parameters like increased stability, absorption characteristics, solubilisation and decreased toxicity, especially in cell-based in vitro assays [23–26]. Since CDs are ‘generally recognized as safe’ (GRAS) by the U.S. Food and Drug Administration (FDA), they are widely used in different industries such as agro-food, cosmetics, pharmacy and chemistry [20,27].

Interestingly, CDs in general and particularly 2-HP- β -CD have not been utilized in assessing in vitro binding affinities of poorly soluble compounds in cell-based GPCR binding assays yet. In general, there is a high need of solubility enhancing approaches for in vitro assays, especially with highly lipophilic test compounds. Due to the attractive properties of 2-HP- β -CD as a solubility enhancer it was used in this case study. The aim of this study was, therefore, to evaluate the impact of IC formation as means of solubility enhancement on D₂R ligand binding affinities in vitro. The dopamine receptor (DR) family was selected as case target because it represents one of the most important GPCR families. With 65 FDA-approved drugs and its involvement in multiple CNS-associated diseases, it acts as a highly relevant proof-of-concept target to investigate 2-HP- β -CD as solubility enhancer in HTRF-based, cell-based assays. [28–32].

2. Materials and methods

2.1. Materials

Apomorphine hydrochloride **1** was a kind gift from EVER Valinjet GmbH (Unterach, Austria). (S)-(–)-sulpiride **2** (S7771-5G, ≥ 98 % (titration)), droperidol **3** (D1414-1G), haloperidol **4** (H0912, >98.0 %), spiperone **5** (S7395-250MG), dimethyl sulfoxide (DMSO, 472301-100ML, ACS reagent, ≥ 99.9 %) and 2-hydroxypropyl- β -cyclodextrin (2-HP- β -CD, H0979) were all acquired from Sigma-Aldrich or TCI Chemicals, Germany. L-(+)-ascorbic acid (L-AA, 011188.A3, 98 %+) was acquired from Alfa Aesar. Tag-lite buffer (TLB, 5X concentrate, 100 mL, stored at 4 °C, LABMED, acquired from PerkinElmer/cisbio) was diluted 1:5 in MilliQ water to generate 1X TLB used throughout solubility studies (see section 2.2) and in vitro studies (see section 2.6). All compounds were stored according to storage conditions provided on the respective data sheets.

2.2. Solubility studies – solvent, incubation time and solubility enhancers

All solubility studies were performed and analysed using a Shimadzu Nexera XR HPLC-DAD (diode array detector) setup. Different isocratic mixtures of MilliQ water +0.1 % trifluoroacetic acid (TFA, suitable for HPLC, ≥ 99.0 %, acquired from Sigma-Aldrich) and acetonitrile (Honeywell, CHROMASOLV™ Plus, for HPLC, ≥ 99.9 %) + 0.1 % TFA were used and individually optimized for each investigated ligand. MilliQ water + 0.1 % TFA is referred to as mobile phase (MP) A. Acetonitrile + 0.1 % TFA is referred to as MP B. Analysis was performed using a Phenomenex Luna® 3 μ m C18(2) 100 Å reversed-phase (RP) column (150 x 4.6 mm). The flow rate was maintained at 1.0 mL/min, column oven and autosampler were set to 35 °C and 25 °C, respectively. All samples and calibration standards were injected in an amount of 50 μ L. Ligand-specific settings are shown in Table 1.

Table 1

Summary of individually optimized HPLC-DAD settings for the investigated ligands. All developed methods represent isocratic methods. Isocratic settings defined via % MP B (acetonitrile + 0.1 % TFA). Wavelength (λ) based on determined absorption maxima in UV-VIS spectra.

Ligand	MP B [%]	λ [nm]	Measurement time [min]
1	25	273	5
2	18	292	
3	38	245	
4	42	246	7
5		248	5

2.2.1. Calibration curves

Original stock solutions (100 mM) were prepared in DMSO. Calibration curves were prepared in MP A (containing max. 1 % DMSO). Calibration standards for **1** and **2** as well as **3**, **4** and **5** included standards with 100/66.7/44.4/29.6/19.8/13.2/8.8/5.9 μM and 10/6.7/4.4/3.0/2.0/1.3/0.9/0.6 μM , respectively. All calibration curves were prepared and analysed using two independent dilution series. Each standard was measured twice resulting in $n = 4$. Calibration curves were analysed calculating goodness of fit (R^2), slope (k), interception (d), standard deviation of the response (σ) limit of detection (LOD) and limit of quantification (LOQ) to ensure statistical validity and reproducibility of the results [33]. LOD [μM], LOQ [μM] and R^2 for each ligand are shown in the following: **1** (0.29, 0.89 and 1), **2** (0.22, 0.68 and 1), **3** (0.29, 0.89 and 0.9994), **4** (0.25, 0.77 and 0.9995) and **5** (0.40, 1.2 and 0.9989).

2.2.2. Solubility studies

Solubility studies were conducted using different solvents (1X TLB assay buffer or Milli Q water), incubation times (0.5 or 48 h) and 2-HP- β -CD concentrations (0 or 40 mM). Each ligand was directly dissolved in the respective solvent with or without (w/o) 40 mM 2-HP- β -CD and incubated for 0.5 or 48 h, respectively.

Solubility studies were performed at 25 °C and 1500 rpm using a thermoblock. After the incubation period, samples were centrifuged for 5 min at 25 °C and 15000 rpm. 100 μL of the supernatants (SN) were transferred into 1.5 mL Eppendorf reaction tubes and diluted in MP A. All solubility studies were performed in three independent replicates with each sample measured twice, resulting in $n = 6$.

Recovery rates [%] of all ligands dissolved in 1X TLB (containing 1 % DMSO) are shown in the following: **1**, 101.8; **2**, 100.1; **3**, 96.5; **4**, 102.6 and **5**, 100.8. Quantified recovery rates were used for method validation and highlighted precision and accuracy of the developed methods.

2.2.3. Phase solubility studies

For phase solubility studies (PSB), ligands **2–5** were dissolved in MilliQ water or 40/20/10/5/2.5/1 [mM] 2-HP- β -CD to achieve theoretical ligand concentrations of 40 mM. Samples were incubated for 48 h (equilibrium) at 25 °C and 1500 rpm. After centrifugation (15000 rpm, 25 °C, 5 min) SNs were diluted in MP A and analysed using the previously described HPLC-DAD setup. 2-HP- β -CD concentration-dependent impact on ligand solubilisation and assessment of A_L -type behaviour was assessed based on phase solubility diagrams proposed by Higuchi and Connors (Fig. 1) [34].

For assessment of B_S -type curves, 2-HP- β -CD concentrations of sample SNs ($n = 3$) were determined using a magritek Spinsolve 60 Carbon NMR device. ^1H spectra were recorded in Proton + mode at 60 MHz and 298 K using 256 scans. The baseline-corrected area of the proton signal of the terminal CH_3 group (duplet) of 2-HP- β -CD at approx. 1.2 ppm was used for quantification. An external 2-HP- β -CD calibration curve (0.5/1.0/2.5/5.0/10/20/40 mM; LOD, 1.02 mM; LOQ, 3.08 mM and R^2 , 0.9996) was used as reference ($n = 2$).

2.3. NMR experiments

All 1D ^1H spectra and 2D ^1H - ^1H NOESY spectra of **1** and **2** were recorded on a Bruker Avance III HD spectrometer operating at 600 MHz equipped with a $^1\text{H}/^{13}\text{C}/^{15}\text{N}/^{31}\text{P}$ QXI probe. 2D ^1H - ^1H NOESY spectra of **3**, **4** and **5** were recorded at on a 700 MHz Bruker Avance III spectrometer with a $^1\text{H}/^{13}\text{C}/^{15}\text{N}$ TCI cryoprobe. All spectra were recorded at 298 K.

2.3.1. Sample preparation and parameters

All samples were prepared in deuterated water (D_2O , 100 atom%D), acquired from ARMAR Chemicals). Samples were prepared at 40 mM and incubated at 25 °C and 1500 rpm (analogous to HPLC solubility studies, see section 2.2.2). After centrifugation at 15000 rpm for 5 min at 25 °C, 650 μL of the SNs were transferred to NMR tubes (Wilmad® NMR

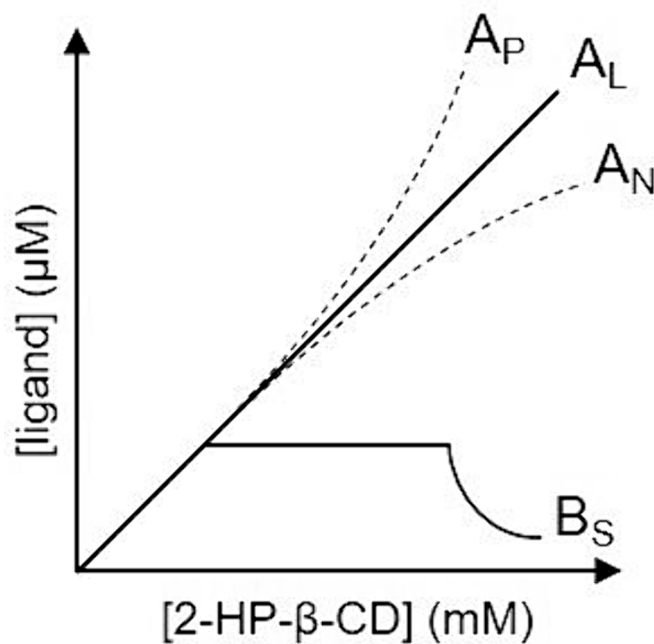


Fig. 1. Overview of IC stoichiometry (drug:CD ratio) based on PSB diagrams. A_L (linear) indicates 1:1 stoichiometry. A_N (negative deviation) indicates ICs of higher order with $\geq 1:1$ stoichiometry. A_P (positive deviation) indicates ICs of higher order with $1:\geq 1$ stoichiometry. B_S curves highlight partially soluble ICs.

tubes 5 mm diam., economy, frequency > 100 MHz, L 7 in.; acquired from Merck). ^1H NMR spectra were recorded for each ligand (free in solution as well as formulated as a 2-HP- β -CD inclusion complex), 2-HP- β -CD in D_2O and 0.1 % L-AA in D_2O .

Unless stated otherwise, 1D ^1H spectra were recorded with 65,536 complex points and a spectral width of 20.0 ppm. The irradiation frequency was adjusted to the remaining water signal. Spectra were processed with an exponential function and a line broadening factor of 0.5. Individual measurement parameters are detailed in Table 2.

For unambiguous assignment of chemical shift values of **3**, TOCSY 2D experiments were acquired with 512 datapoints in F1 and 2048 datapoints in the F2 dimension and a spectral width of 11 ppm in each dimension. A mixing time of 80 ms was used. For acquisition, 128 dummy scans were used to equilibrate the system prior to actual 8 scans per measurement. For increased S/N ratio, 8 individual spectra were collected consecutively and accumulated into a new 2D TOCSY spectrum.

2D ^1H - ^1H NOESY were acquired with 2048 x 600 complex points for **1** and **2** and with 2048 x 512 complex points regarding **3–5**. Ligand **1** and **2**, **3** and **4** and ligand **5** spectra were recorded using 88, 64 and 56 transients, respectively. Mixing time was 120 ms for all ligands.

Table 2

Acquisition and processing parameters for ligands **1–5** as well as 2-HP- β -CD and L-AA. Parameters show settings for 'free' ligands and IC formulated ligands.

Ligand	1		2		2-HP- β -CD		L-AA
Parameter	'free'	IC	'free'	IC			
NS	1			32	1		16
Recycle delay [sec]	1.000			5.000	1.000		3.000
Ligand	3		4		5		
Parameter	'free'	IC	'free'	IC	'free'	IC	
NS	896	64	640	64	640	64	
Recycle delay [sec]	5.000						

2.3.2. Analysis of ^1H shifts

^1H proton spectra were processed and analysed with Topspin 3.6.2 (Bruker, Billerica, MA, USA). Annotation of 2-HP- β -CD protons was based on the work by Yang and colleagues detailing the frequencies [ppm] of H_1 to H_6 considering the monomeric glucose subunits (α -1,4-glycosidic bonds) of 2-HP- β -CD in D_2O [35]. The formation of ligand – 2-HP- β -CD inclusion complexes was assessed based on ^1H shifts of ligand protons (exemplified by Hao et al. in [26]), since 2-HP- β -CD ^1H signals were too dominant due to high concentrations (40 mM) used in the experiments. Chemical shift assignments were derived either from 2D NMR correlations or by comparison of spectra including coupling patterns with previously published NMR data [36–40]. The solvent residual peak of HDO was set to 4.79 ppm to allow for better comparability between different ^1H spectra [41].

2.4. Basin hopping global optimization of IC structures (in silico studies)

In order to propose energetically favourable IC structures, a basin hopping global minimization study was performed using ligands 1–5 (including two agonists and three antagonists) [42]. The starting structures were generated by placing a single ligand molecule into the cavity of a pre-optimized β -CD. Next, the ligand was rotated along the x, y and z-axes in intervals ranging from 0 to 180° in 15° steps, respectively. In addition, a horizontal shift out of the β -CD plane was considered. For the smaller compound 1, shifts in the range from -1.0 to 1.0 \AA in steps of 0.5 \AA were performed, whereas an increased range from -3.0 to 3.0 \AA with increments of 1.0 \AA was used in all other cases. This resulted in 10,985 and 15,379 individual starting structures for the small and large substrate molecules, which were then subjected to a distance-based pre-selection (minimum host–guest atom-distance $r_{\text{min}} \geq 0.9 \text{ \AA}$).

In the first step, a pre-optimisation using the recently developed ANI-2x neural network potential (NNP) was carried out [43]. Based on the resulting interaction potential, the ten best conformations of each substrate were then subject to further minimisation at self-consistent charge density functional tight binding (SCC DFTB) level [44] employing the DFTB+ program [45] using the 3ob parameter set [46–48] and D3 dispersion correction [49]. In order to account for the influence of solvation effects, the conductor-like screening model (COSMO) [50] was applied and the five conformers with the lowest interaction energy were selected for further analysis. Visualization was carried out using VMD [51]. All calculations were performed considering a 1:1 ratio of the host (β -CD) and guest (ligands 1–5) species. Ligand binding modes and

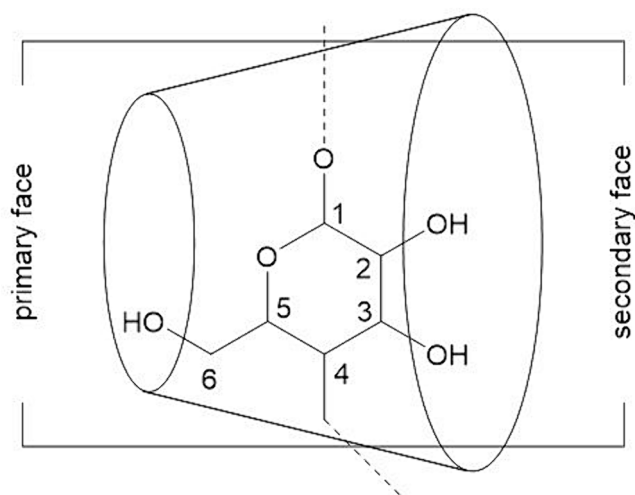


Fig. 2. Overview of the β -CD cavity geometry (based on [52]) showing the orientation of one glucose monomeric subunit with C_6 facing towards the primary face (smaller diameter) and C_2 and C_3 facing towards the secondary face (wider diameter). Created with BioRender.com.

interactions with the primary and secondary face OH groups of CD were based on the cavity geometry shown in Fig. 2 [52].

Optimizations were performed at 0 K, thus, neglecting entropic effects. β -CD instead of 2-HP- β -CD was used due to unknown degree of substitution of 2-HP- β -CD. Regarding the considerable impact of different 2-HP- β -CD substitution patterns on IC formation and stoichiometry as well as ligand binding mode, β -CD was considered to generate more robust and reproducible simulations results [53–56].

2.5. Cytotoxicity CellTiter blue (CTB) assay

Human embryonic kidney (HEK) 293T cells (kindly provided by the research group of Angelika Vollmer, department of Pharmaceutical Biology, LMU Munich; originally acquired from ATCC, CRL-3216) were cultivated in high glucose DMEM (Dulbeccó's Modified Eagle Medium, 4.5 g/L glucose, w/o L-glutamine and 3.7 g/L NaHCO_3 ; acquired from PAN-biotech) containing 10 % fetal bovine serum (FBS superior, S0615; acquired from Sigma-Aldrich) and 1x penicillin/streptomycin (P/S, 100x concentrated; acquired from PAN-biotech). All cell culture flasks/multi-well plates used during cultivation and cytotoxicity tests were pre-coated with a PBS/collagen mixture (0.001 %) for 15 min at 37°C and 5 % CO_2 . Cells were cultivated at 37°C , 5 % CO_2 and constant humidity.

Cells used for CTB measurements were taken during passaging of HEK293T cells. CTB measurements were performed in 96-well plates (BioLite 96 Well Multidish, transparent, flat bottom, acquired from ThermoScientific) using 100,000 cells per well (in a volume of 200 μL). During passaging, the appropriate volume of cell suspension (containing 500,000 cells/mL) was diluted in fresh DMEM. 200 μL of cell suspension was transferred to each well. Cells were incubated for 24 h. After 24 h incubation, medium was discarded and cells were treated with 100 μL of DMEM (control), 1 % DMSO (in DMEM) or 40/20/10/5/2.5/1 mM of 2-HP- β -CD (treatment) for 3 h (representative of the total duration of the cell-based HTRF assay, see section 2.6). After incubation (37°C , 5 % CO_2) 10 μL of CellTiter-Blue® (CTB, cell viability assay, acquired from Promega) were added to each well. Cells were incubated for 5 h. After incubation, fluorescence (random fluorescence units (RFU)) of each well was measured using a Tecan Spark plate reader (Tecan Group, Männedorf, Switzerland). 96-well plate was shaken for 5 s at 1440 rpm prior to measurement. Excitation/emission wavelengths were set to 560 and 590 nm using monochromators with 20 nm bandwidth. CTB measurements were performed in three biological replicates (at p15, p16 and p19) using three technical replicates, resulting in $n = 9$ for each tested condition. Additionally, a cytotoxicity control (Lysis Solution, 10X, G182B; acquired from Promega) was used. RFU values were normalized against the control.

2.6. In vitro D_2R binding affinity based on a cell-based HTRF assay

In vitro studies determining the binding affinity of the investigated ligands with and w/o the use of 2-HP- β -CD were performed using D_2R -expressing cells (Tag-lite Dopamine D_2 -labelled Cells, ready-to-use, transformed and labelled, 200 tests, C1TT1D2) acquired from PerkinElmer/cisbio. Fluorescent ligand (Dopamine D_2 Receptor red antagonist Fluorescent Ligand, stored at -20°C , L0002RED), assay buffer (Tag-lite Buffer, 5X concentrate, 100 mL, stored at 4°C , LABMED) and 96-well plates (HTRF 96-well low-volume white plate, 66PL96005) were all acquired from PerkinElmer/cisbio. Setup details relevant for the measurement as well as characterization of the D_2R carrier cells are described in Zell et al. [57].

2.6.1. Preparation of ligand solutions

Ligand solutions were prepared based on solid compounds to avoid use of DMSO. Two independent samples for each ligand and condition were weighed in and dissolved in 1X TLB with or w/o 40 mM 2-HP- β -CD achieving theoretical ligand concentrations of 40 mM (solutions of 1 contained 0.1 % L-AA for stability reasons). Ligands were incubated for

30 min at 1500 rpm and 25 °C. After centrifugation, SNs were transferred and immediately used for subsequent K_i determination. SNs were diluted prior to determination of K_i values, resulting in maximum 2-HP- β -CD concentrations of 1 mM. During K_i determination (2 h incubation period), ligand concentrations in each sample were quantified with HPLC (see section 2.2).

2.6.2. Determination of biological binding affinities

In vitro binding affinities of ligands 1–5 were determined using the SOP provided by cisbio/PerkinElmer. In brief, ligand solutions were diluted in 1X TLB to generate a standard dilution series. Two individual series were prepared for each ligand with and w/o 2-HP- β -CD, totalling a number of $n = 4$. Fluorescence-labelled ligand was diluted in 1X TLB at four times of the determined K_d value of the D₂R carrier cells ($K_d = 39.09$ nM). D₂R carrier cells were prepared in 1X TLB according to the SOP and distributed to two 96-well plates (10 μ L/well). Each concentration of the dilution series was tested with $n = 3$ (5 μ L/well). Additionally, blank values including 1X TLB, 1X TLB + 0.1 % L-AA and 2-HP- β -CD at different concentrations were included to ensure assay functionality. Labelled ligand was dispensed to each well (5 μ L/well). Plates were incubated for 2 h in a styrofoam box for exclusion of light and constant temperature and subsequently measured using a Tecan Spark plate reader. K_i calculations were based on exact ligand concentrations determined with HPLC.

2.6.3. Data Processing, representation and analysis

Statistical analysis was performed in GraphPad Prism 8.2.1 (GraphPad Software, San Diego, CA, USA). Saturation binding curves were analysed using ‘Nonlinear regression (curve fit), One site—Fit logIC50’.

Bar charts regarding solubility, cytotoxicity, HTRF assay functionality and K_i comparison were analysed using ‘Ordinary one-way ANOVA (Sidak)’ and ‘Unpaired t -test (parametric, two-tailed)’. NMR spectra were assessed using Bruker TopSpin 3.6.2 (Bruker, Billerica, MA, USA). 2D structures of all shown compounds were generated using ChemDraw version 19.0 (PerkinElmer, Waltham, MA, USA).

3. Results

3.1. Solubility studies

Solubility studies showed significant solubility enhancing effects of 2-HP- β -CD under different conditions. Quantified concentrations of 1–5 are summarized in Fig. 3A–E.

Fig. 3A shows that only 1 fully dissolved in MilliQ water (both with and w/o 2-HP- β -CD and after 0.5 and 48 h) reaching the maximum achievable concentration of 40 mM. In contrast, ligands 2–5 reached maximum concentrations of 7482.4 μ M (2, 18.7 % recovery), 464.3 μ M (3, 1.2 % recovery), 447.7 μ M (4, 1.1 % recovery) and 231.7 μ M (5, 0.6 % recovery), respectively. In the presence of 40 mM 2-HP- β -CD, 1 and 3 both achieved maximum concentrations in aqueous (MilliQ water) conditions, while 2, 4 and 5 were most soluble in 1X TLB. However, all ligands showed significantly increased solubility in 1X TLB with 40 mM 2-HP- β -CD after 0.5 h of incubation compared to 1X TLB conditions without (w/o) 2-HP- β -CD. Solubility enhancing effects of 2-HP- β -CD were observed in all conditions (Table 3).

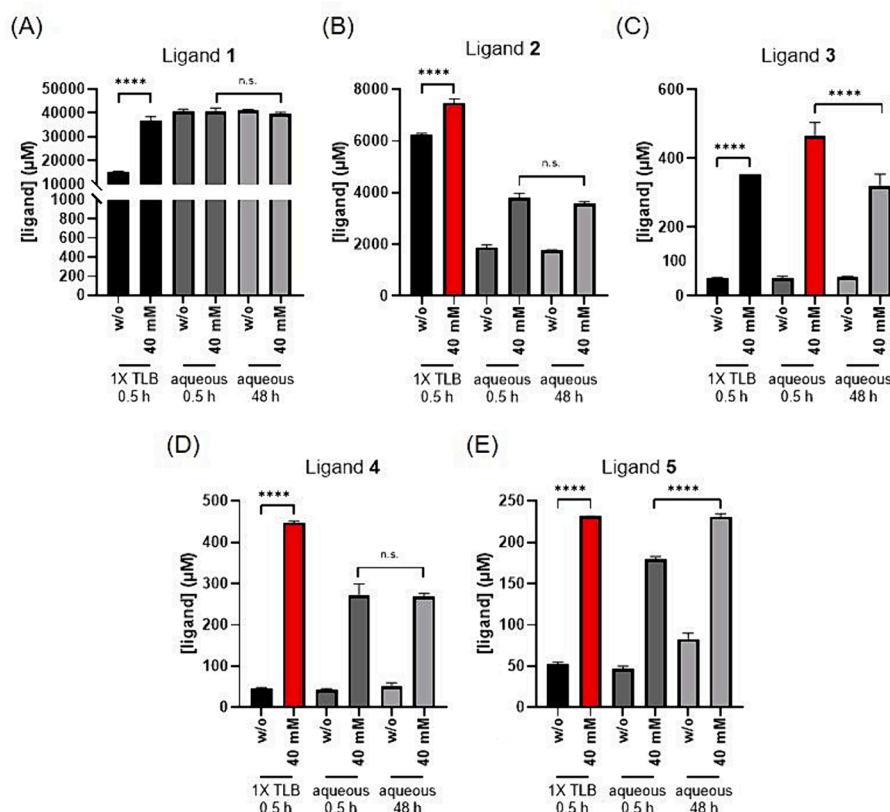


Fig. 3. Ligand solubility comparing different solvents, incubation periods and the use of 2-HP- β -CD as a solubility enhancer. The determined concentrations of (A – E) 1–5 are shown in 1X TLB (black bars), MilliQ water after 0.5 h (dark grey bars) and after 48 h (light grey bars) for three independent replicates (each measured twice), resulting in $n = 6$. Bars show SD values. Ideal conditions are highlighted in red. X-axes show used 2-HP- β -CD concentrations. Y-axes display different ranges due to the different solubilities of the investigated ligands. Graphs were visualized and statistically analysed (ordinary one-way ANOVA, Sidak) in GraphPad Prism 8.2.1. n.s., not significant. **** $p < 0.0001$. (For interpretation of the references to colour in this figure legend, the reader is referred to the web version of this article.)

Table 3

Solubility enhancement factor (x-fold) based on quantified ligand concentrations assessing impact of 2-HP- β -CD using different solvents and incubation periods. Ligand concentrations were determined with $n = 6$. inc., incubation.

Ligand	x-fold ^a (comparing with and w/o 2-HP- β -CD)		
	1X TLB	Milli Q (0.5 h inc.)	Milli Q (48 h inc.)
1	2.4	1.0	0.95
2	1.1	1.6	2
3	6.7	8.9	5.8
4	9.6	6.5	5.3
5	4.4	3.8	2.8

^a Solubility enhancement factors (x-fold) were calculated in reference to quantified concentrations without using 2-HP- β -CD. Values > 1 indicated increased solubility using 2-HP- β -CD.

3.2. Phase solubility studies (PSBs)

The formation of ICs was quantitatively assessed based on determined ligand concentrations. A_L-type behaviour indicative of a 1:1 stoichiometry and higher-order guest:host stoichiometries (e.g. 1:2) were assessed (originally proposed by Higuchi and Connors and exemplified in previous work by Saokham et al (shown in Fig. 1) and Loftsson and colleagues [34,58,59]).

The resulting correlations are shown in Fig. 4A–D. Ligand 1 was not investigated due to full solubility in aqueous and 40 mM 2-HP- β -CD conditions.

Concentrations of ligands 2 and 4 increased linearly with increasing 2-HP- β -CD concentrations, indicating a 1:1 stoichiometry (Fig. 4A and C, black circles). Ligands 3 and 5 showed a different, clearly non-linear behaviour with increasing 2-HP- β -CD concentrations (Fig. 4B and D, black circles). The B_S-type behaviour indicates a 1:1 stoichiometry at lower 2-HP- β -CD concentrations (≤ 10 mM and ≤ 1 mM for ligands 3 and 5, respectively), while the solubility limits of the generated ICs are approached at higher concentrations. Formation of insoluble ligand 3 and 5 ICs was shown by decreased 2-HP- β -CD concentrations (Fig. 4B

and D, black squares) in the sample SNs (compared to 2-HP- β -CD concentrations used for IC generation, shown on x-axis). Ligand 3 and 5 ICs for B_S-type assessment were generated using 5, 10 and 20 mM 2-HP- β -CD. Ligand 3 sample SNs yielded 2.31 ± 0.03 , 4.82 ± 0.06 and 10.00 ± 0.02 mM, respectively. Ligand 5 sample SNs resulted in only 2.38 ± 0.12 , 4.98 ± 0.23 and 10.27 ± 0.12 mM, respectively, after 48 h incubation.

3.3. NMR experiments

3.3.1. Formation of ligand ICs

To further assess the formation of ligand – 2-HP- β -CD ICs, aromatic proton chemical shift deviations upon IC formation were analysed. The ¹H signals of 2-HP- β -CD are shown in Fig. 5A to enable discrimination of ligand signals in IC formulations. In Fig. 5B–F the superpositioned NMR spectra of ‘free’ (red) and IC formulated (blue) ligands 1–5 are shown. Peak annotations are additionally shown in reference to the 2D structure.

Observed aromatic proton chemical shift deviations for ligands 1–5 are shown in Table 4. Downfield (shown by a negative delta Δ) and upfield shifts (shown by a positive delta Δ) of aromatic protons highlight changes of the ligands chemical environment due to intrusion into the 2-HP- β -CD cavity. Additionally, downfield shifts indicated deshielding of protons due to hydrogen bond (HB) formation of neighbouring donor- and acceptor groups with 2-HP- β -CD in IC formation [60].

Proton signals d and e of 1 (Fig. 5B) fused and generated a single signal upon IC formation. Signals originating from protons b, c and d of 3 (Fig. 5D) formed a complex multiplet in ‘free’ conditions. Interestingly, upon IC formation, the multiplet split up into a distinct pseudo-triplet (dd with ³J_{HP} and ³J_{HH} being very similar) (b’), a duplet (c’) and another multiplet (d’). Proton signal b appeared as a pseudo-triplet due to similar coupling constants with the neighbouring proton a and the neighbouring *para*-substituted fluorine. Proton signal d of 4 (Fig. 5E) appeared as a pseudo-triplet due to similar coupling constants with the neighbouring proton a and the neighbouring *para*-substituted fluorine.

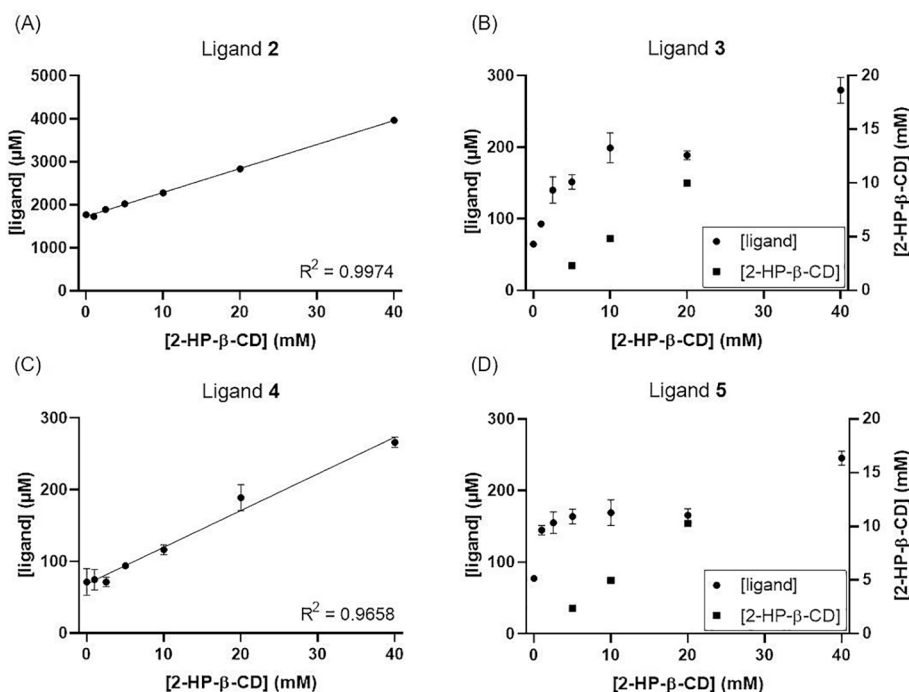


Fig. 4. Overview of phase solubility studies of ligands 2–5. (A–D) Determined concentrations [μ M] of 2–5 (black circles, primary y-axis) after 48 h incubation using different 2-HP- β -CD concentrations [mM] assessing IC stoichiometry. Three independent samples were prepared for each concentration and measured twice, resulting in $n = 6$. (B + D) Quantified 2-HP- β -CD concentrations ($n = 3$) in sample supernatants (black squares, secondary y-axis) assessing formation of insoluble ICs. Concentrations [μ M and mM] are shown \pm SD. 2-HP- β -CD concentrations used during incubation are shown on the x-axis.

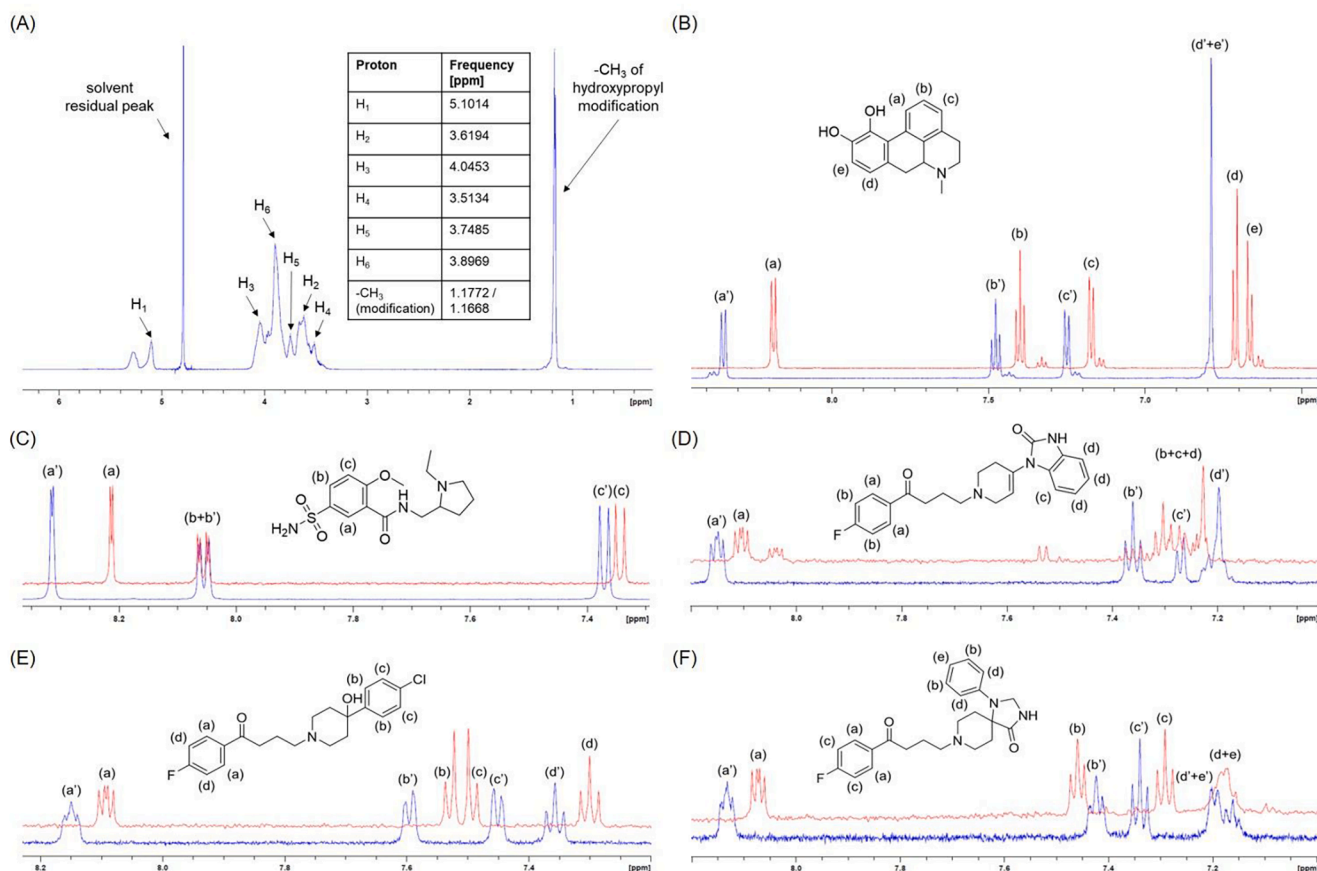


Fig. 5. Overview of the ^1H NMR spectra of (A) 2-HP- β -CD (40 mM), with peak annotation based on Yang and colleagues [35] and (B–F) ligands 1–5 comparing signals of ‘free’ ligand (red) and IC formulation (blue). Letters highlight peaks originating from the same protons in the different formulations. 2D structures of 1–5 are shown with letter-based annotation in reference to the NMR signals. Spectra were analysed and processed in Bruker TopSpin 3.6.2. (For interpretation of the references to colour in this figure legend, the reader is referred to the web version of this article.)

Table 4

Summary of aromatic ^1H proton signals [ppm] recorded during NMR experiments. Signal deviations Δ [ppm] were calculated in reference to the ‘free’ signal. In case of duplets, triplets, multiplets, etc., mean [ppm] for all peaks of an individual signal were used to simplify comparisons. Negative Δ indicate downfield shifts of ^1H signal(s) due to IC formation. Positive Δ indicate upfield shifts ^1H signal(s) due to IC formation. Proton annotations are based on Fig. 5.

Ligand	Chemical shift deviations (Δ ppm) for aromatic protons				
	a	b	c	d	e
1	−0.16	−0.08	−0.08	−0.08	−0.10
2	−0.11	0.00	−0.03	–	–
3	−0.05	−0.06	0.03	0.10	–
4	−0.06	−0.07	0.04	−0.06	–
5	−0.06	0.03	−0.05	0.00	0.00

Ligand 5 proton signals (Fig. 5F) originating from d and e appeared to remain mainly unaffected even though the signals separated slightly. Proton signal c appeared as a pseudo-triplet due to similar coupling constants with the neighbouring proton a and the neighbouring *para*-substituted fluorine as in ligands 3 and 4.

3.3.2. Binding modes of ligands in IC cavities

In addition to the assessment of IC formation based on ^1H NMR spectra, 2D NMR experiments were performed investigating intermolecular NOE correlations between ligands 1–5 elucidating binding modes within the 2-HP- β -CD cavity. 2D ^1H - ^1H NOESY spectra of 1–5 are shown in Fig. 6A–E, respectively.

The NOESY spectrum of ligand 1 (Fig. 6A) showed intermolecular

NOE correlations between aromatic proton signals d and e (and weakly signal a) with both H3 and H5. Aromatic signals b and c didn’t show any correlations with 2-HP- β -CD. Those results strongly indicated a unique binding mode of 1 with the catechol moiety (adjacent to signals d and e) protruding deep into the cavity, while the bulkier part of 1 (containing signals a, b and c) protrudes towards the exterior. All aromatic proton signals of ligands 2 and 4 (Fig. 6F and D) showed intermolecular NOE correlations with both H3 and H5, suggesting a deep intrusion of the ligands into the cavity. All aromatic signals of 3 and 5 (Fig. 6C and E) showed correlations with 2-HP- β -CDs H5. Proton signal d of 3 showed additional intermolecular interactions with H3 (Fig. 6C). In addition, ligand 5 aromatic proton signals a, b and c (but not d or e) showed NOE correlations with H3 (Fig. 6E).

Ligand 2 signals b and c were characterized by two distinct NMR signals each. All the other aromatic proton signals of 2–5 showed characteristic broadening (in contrast to the sharp signal of 1). Split or broadened NOESY signals were indicative of two different binding modes of ligands 2–5 within the 2-HP- β -CD cavity after IC formation.

3.4. Basin hopping global optimization

In silico simulations were performed to elucidate possible binding modes of ligands 1–5 upon IC formation with 2-HP- β -CD (Fig. 7A–E). Binding complexes were visualized observing the cavity from the top (left panel) and side (middle panel). Additionally, 2D ligand structures are shown in a similar position as in the side view to allow for easier comparison (right panel).

Ligand 1 (Fig. 7A) protruded deep into the cavity of β -CD with its

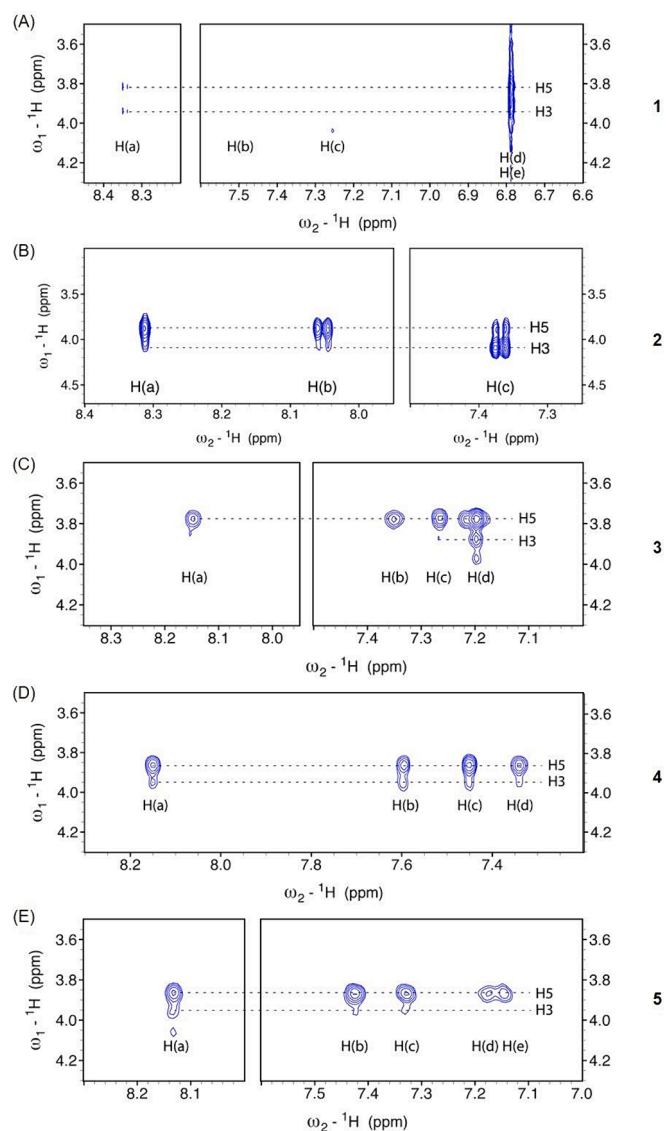


Fig. 6. 2D ^1H - ^1H NOESY NMR spectra of ligands 1–5 (A – E), highlighting intermolecular interactions between the ligands aromatic protons and H3 and H5 proton signals of 2-HP- β -CD. X- and y-axes show ligand aromatic and 2-HP- β -CD proton signals [ppm], respectively.

catechol moiety oriented towards the primary face. The bulky tetracyclic scaffold of **1** entered the cavity almost completely with the tertiary amine oriented towards the secondary face, thus, residing within the wider part of the cavity. A HB was formed between the *para*-OH group of the catechol moiety of **1** and the C₆-OH group from β -CD (primary face). The interaction energy of the formed complex was determined as -166.7 kJ/mol.

Ligand **2** (Fig. 7B) entered the cavity deeply with its sulfonamide moiety exiting the ring-like structure of β -CD at the primary face. The sulfonamide motif formed a HB with the C₆ OH group of the primary face. The oxygen atom of the amide acted as a HBD forming HBs with C₁- and C₅ OH groups of two different glucose subunits. The pyrrolidine moiety protruded slightly from the secondary face. The interaction energy of the formed complex was determined as -192.0 kJ/mol.

The benzimidazole moiety of ligand **3** (Fig. 7C) as well as the tetrahydropyridine motif completely entered the cavity oriented towards the primary face. The fluoro-substituted aromatic ring with adjacent carbonyl group was protruding from the cavity at the side of the secondary face. Based on the *in silico* simulations no HBs were formed between **3** and the OH-groups of β -CD. The interaction energy of the

formed complex was determined as -195.2 kJ/mol.

Ligand **4** (Fig. 7D) was characterized by aromatic, lipophilic structural motifs at both ends. The chlorine-substituted aromatic ring entered the β -CD cavity protruding towards the primary face. The aliphatic linker region as well as the piperidine moiety resided centrally within the cavity. The carbonyl group and the fluorine-substituted aromatic ring exited the cavity at the secondary face. However, the bond angle between C₂, C₃ and C₄ of the aliphatic linker approximated a 90° angle, thus, the aromatic motif was flipped towards the secondary face. The binding mode was stabilized by two HBs formed between the carbonyl oxygen and C₂- and C₃ OH groups of one glucose subunit of the secondary face. The interaction energy of the formed complex was determined as -215.9 kJ/mol.

While ligand **5** (Fig. 7E) is structurally related to **3** and **4** (butyrophenone-derivatives), its orientation within the cavity was flipped horizontally. The fluoro-substituted aromatic ring and the adjacent carbonyl motif were oriented towards the primary face. In contrast, its 1,3,8-triazospiro[4.5]decan-4-one moiety was sitting centrally within the cavity orienting itself towards the secondary face. The attached phenyl ring was already protruding from the cavity at the side of the secondary face. Analogous to **3**, no HBs were shown in the *in silico* simulation. The interaction energy of the formed complex was determined as -199.3 kJ/mol.

3.5. Cytotoxicity studies

Because a cell-based (HEK293T cells representing the cellular background) *in vitro* assay was used for the determination of ligand binding, it was essential to investigate if 2-HP- β -CD alone had an impact on cellular integrity. Cytotoxicity assays investigating the impact of different concentrations of 2-HP- β -CD on cell viability (see Fig. 8) were performed using the CellTiter blue (CTB) assay.

HEK293T cells showed significantly decreased viability after incubation with 10, 20 and 40 mM 2-HP- β -CD as well as lysis buffer (toxicity control) with adjusted p-values of <0.0001 . Incubation with 1, 2.5 and 5 mM 2-HP- β -CD resulted in no significant decrease in cell viability compared to control cells (treated with medium only).

3.6. *In vitro* binding affinity studies

To investigate the effect of IC formulation on *in vitro* binding affinity, K_i values of 1–5 (detailed in Fig. 9 and Fig. 10 as well as in Table 5) were determined with and w/o 2-HP- β -CD (different concentrations). Ligands were dissolved in 1X TLB with and w/o 2-HP- β -CD to achieve maximum theoretical concentrations of 40 mM. To ensure assay functionality, the effect of a 2-HP- β -CD dilution series regarding the HTRF assays fluorescence signal was investigated (Fig. 9).

2-HP- β -CD concentrations of 0.25 and 0.625 mM didn't show significantly decreased fluorescence values (specific signal) compared to control wells. At ≥ 1 mM specific signals significantly decreased concentration-dependent. A concentration of 1 mM 2-HP- β -CD was the highest concentration present during K_i determinations of ligands 1–5 (Fig. 10 and Fig. 11).

A summary of concentration–response curves of ligands **1** and **3–5** for each tested condition is shown in Fig. 10A–D. Additionally, mean K_i values for each ligand and condition (n = 6) were determined and compared using an unpaired *t*-test to calculate statistical differences between the different conditions (Fig. 10E–H).

Ligands **1** and **3** didn't show statistically significant differences determining K_i values with or w/o 2-HP- β -CD. However, ligands **4** and **5** did show significantly decreased binding affinities (increased K_i values) under IC conditions, highlighting a ligand-specific effect of 2-HP- β -CD complex affecting binding affinities.

To rule out cytotoxic or cell lytic effects of 2-HP- β -CD at higher concentrations impacting assay functionality and affecting biological binding affinities, ligand **2** was investigated using two different 2-HP-

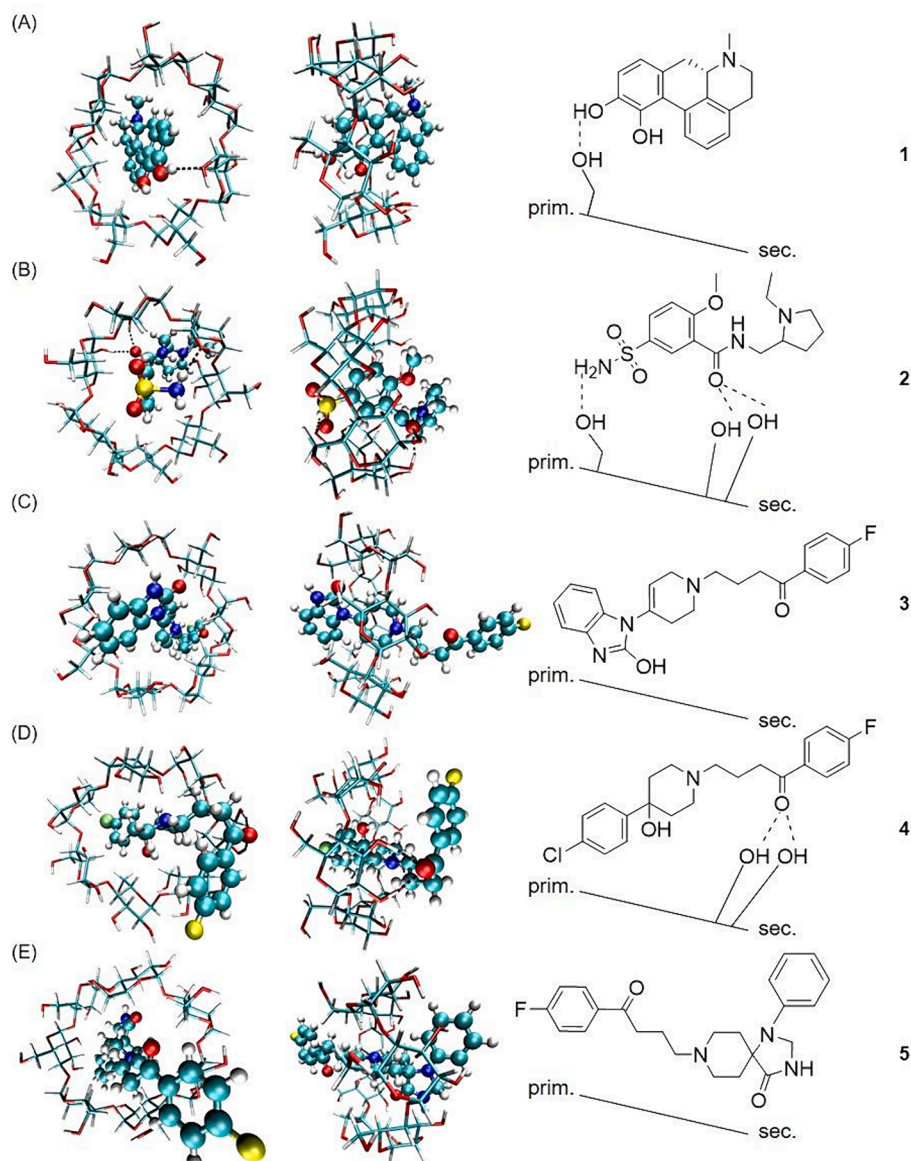


Fig. 7. In silico simulations of ligands 1–5 (A – E) binding within the cavity of β -CD using a basin hopping global minimization process. Primary/secondary face birds-eye view of the ICs and side views with the primary face oriented to the left are shown in the left and middle panel, respectively. 2D structures of ligands 1–5 with intermolecular interaction(s) between ligands and β -CD are shown in the right panel with dashed lines indicating HBs. prim., primary face. sec., secondary face.

β -CD concentrations (Fig. 11).

No statistically significant differences in K_i values were observed using a maximal concentration of 1 mM 2-HP- β -CD, ruling out general cytotoxic effects causing the reduced affinity of 4 and 5 (see Fig. 10), respectively. All determined K_i values (mean values for each tested condition) are additionally summarized in Table 5.

4. Discussion

The results outlined above clearly highlight the solubility enhancing capacities of 2-HP- β -CD for all investigated ligands in a ligand-independent manner. Ligands 1 and 2 represent well water-soluble compounds (aqueous saturation concentrations of 40.5 ± 1.1 and 1.9 ± 0.09 mM), while ligands 3–5 only achieved maximum concentrations of 51.9 ± 4.2 and 41.7 ± 3.7 to 47.0 ± 3.1 μ M, respectively. 2-HP- β -CD increased the solubility of all ligands (except 1, which was already completely soluble in aqueous conditions) in assay (1X TLB) and aqueous conditions (Fig. 3). Under in vitro assay buffer conditions, the solubility of ligands 1 and 2 increased only slightly by factors of 2.4 and

1.1, respectively. Ligands 3–5 benefitted by 6.7-, 9.6- and 6.4-fold increased solubilities.

NMR studies suggested IC formation, which was indicated by shifts of aromatic proton signals (shown in Fig. 5). Such shifts implicate intrusion of the ligand into the CD cavity [26]. Compound 1, which was fully soluble under aqueous conditions, was characterized by prominent proton signal deviations in the aromatic range. Therefore, also 1 preferentially interacts with CD generating an IC. This was also suggested by in silico studies showing an IC overall negative binding energy. Ligands 2–5, all exerting a significantly lower aqueous solubility compared to 1, were characterized by lower overall binding enthalpies, thus, pointing towards preferential IC formation. Again, this was in accordance with the quantified solubility enhancement factors (shown in Table 3), where ligands 2–5 were characterized by a more pronounced impact on in vitro solubility (higher x-fold) using 2-HP- β -CD in comparison to 1 and 2. Consequently, in silico simulations and solubility results were in accordance, suggesting that the encapsulation of ligands with lower aqueous solubility in the β -CD cavity was energetically favourable.

Additionally, in silico simulations (Fig. 7) showed the generation of

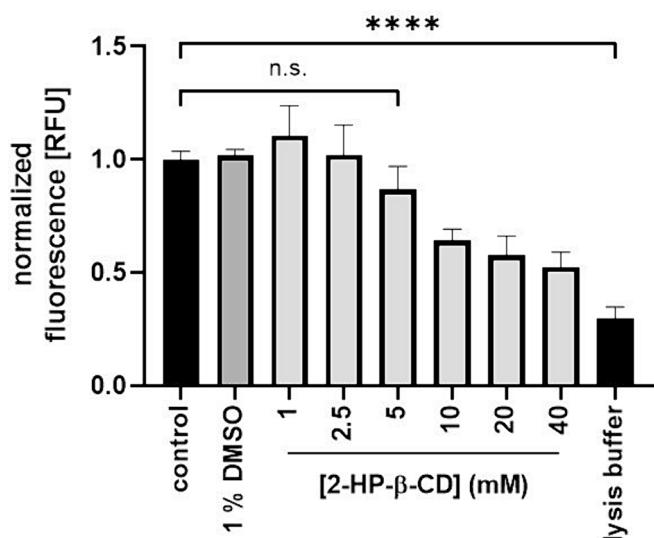


Fig. 8. The effect of different 2-HP- β -CD concentrations on HEK293T cell viability assessed by CTB cytotoxicity assay in comparison to the control (medium only). Normalized fluorescence [RFU] values (y-axis) are shown for $n = 9$ (three biological replicates with three technical replicates each) including \pm SD. Statistical analysis was performed using ordinary one-way ANOVA (Sidak) in GraphPad Prism 8.2.1. n.s., not significant. **** $p < 0.0001$.

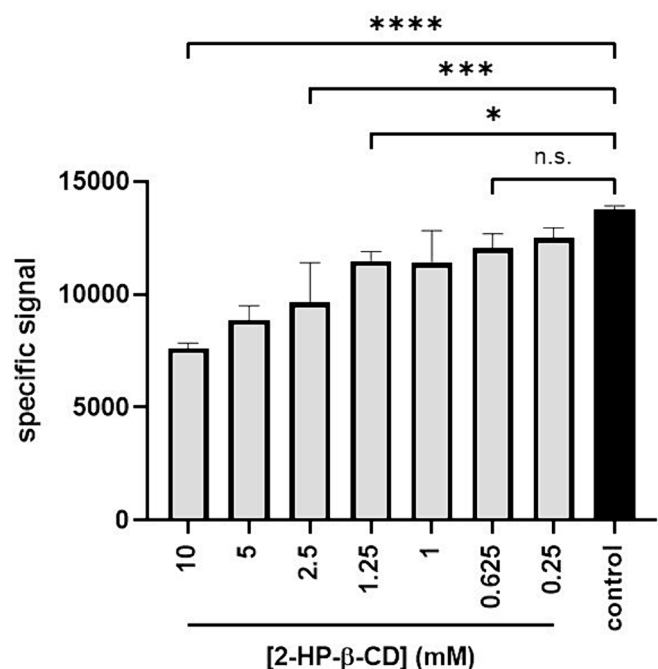


Fig. 9. Effect of different 2-HP- β -CD concentrations on the specific signal fluorescence output of the cell-based homogenously time-resolved fluorescence (HTRF) assay in comparison to the control (only buffer). Concentrations are representative of 2-HP- β -CD concentrations present during Ki determination of ligands 1–5. Each concentration was investigated using technical triplicates. Statistical analysis was performed using ordinary one-way ANOVA (Sidak) in GraphPad Prism 8.2.1. n.s., not significant. **** $p < 0.0001$. *** $p = 0.0002$. * $p = 0.0335$ and 0.0275 , respectively.

HBs between OH-groups from the primary and/or secondary face of CD and donor/acceptor features of the ligands. Since the generation of HBs deshields neighbouring protons, those particular shift intensities were assessed. Proton signals a and e of **1** experienced the most intense downfield shifts (-0.16 and -0.12 ppm). Both of them are closest to the

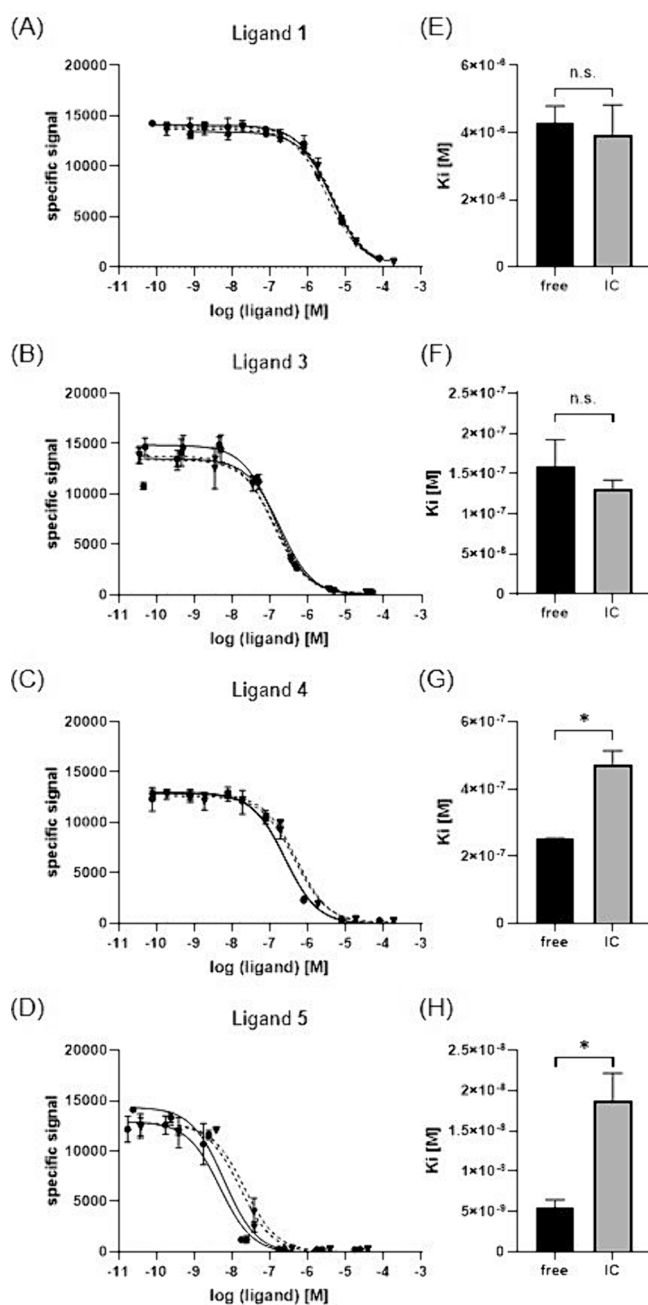


Fig. 10. Determination of binding affinities (K_i) comparing ligands 1 and 3–5 prepared in 1X TLB buffer with or w/o 40 mM 2-HP- β -CD. (A–D) Dose-response curves for ‘free’ (continuous lines) and IC formulated ligands (broken lines) as well as (E–H) statistical comparison of K_i values are shown. K_i values were determined for two independent replicates for each condition (using technical triplicates) resulting in $n = 6$. Determined K_i values were compared using a t -test testing GraphPad Prism 8.2.1. n.s., not significant. * $p = 0.0152$ and 0.0336 .

catechol moiety of **1**, forming a HB with the primary face. Regarding ligand **2**, especially proton signal a was affected by a major downfield shift of -0.10 ppm. Since proton a is positioned between the sulfonamide- and the amide moiety of **2**, which are both involved in HB generation with either the primary or secondary CD face, this shift is expected. Ligand **4** is characterised by a slightly different behaviour. While proton signal b experienced the strongest upfield shift (-0.07 ppm), no HB generation is shown in its vicinity during in silico simulations. However, the chloro-substituted aromatic ring is deeply

Table 5

Summary of K_i values determined for ligands 1–5 in vitro using a cell-based HTRF assay. Values result from $n = 6$ measurements. X-fold values are calculated in reference to 'free' K_i values.

Ligand	K_i (free) \pm SD [μ M]	K_i (IC) \pm SD [μ M]	x-fold
1	4.285 \pm 0.51	3.947 \pm 0.89	1.09
2	0.0976 \pm 0.0071 ^a	0.0962 \pm 0.010 ^a	1.01
3	0.158 \pm 0.034	0.130 \pm 0.012	1.22
4	0.252 \pm 0.012	0.474 \pm 0.39	0.53
5	0.00548 \pm 0.00097	0.0187 \pm 0.0034	0.29

^a K_i values determined using 0.2 mM 2-HP- β -CD.

^b K_i values determined using 1.0 mM 2-HP- β -CD.

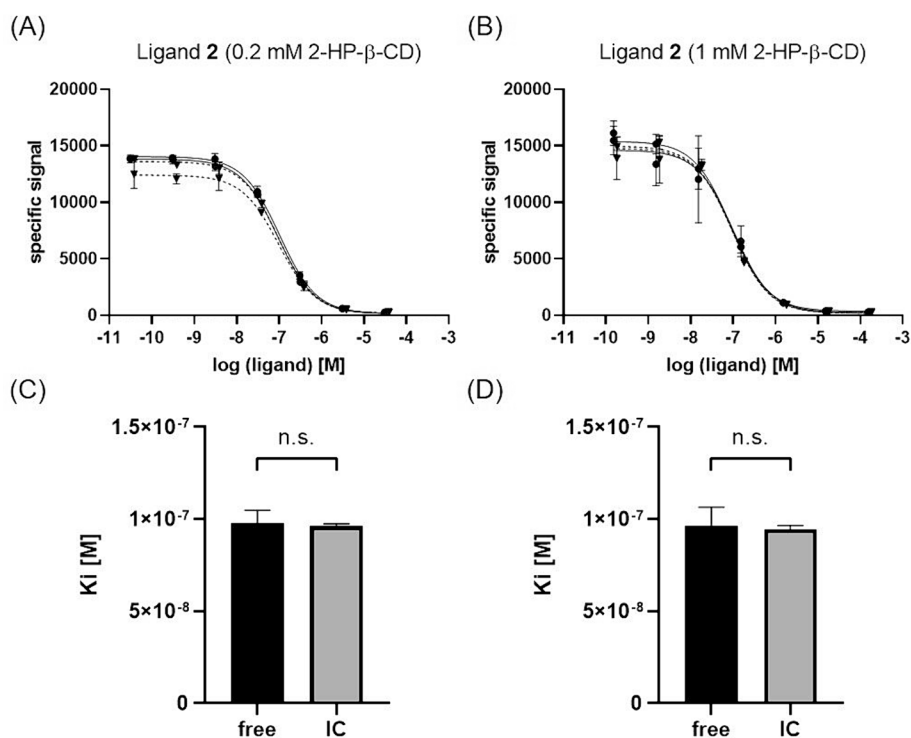


Fig. 11. Comparison of K_i values of 2, using different 2-HP- β -CD concentrations during the in vitro assessment. Dose-response curves for (A) 0.2 mM and (B) 1 mM 2-HP- β -CD as well as bar charts comparing the corresponding K_i values (C) and (D) are shown. Each condition was tested using two independent biological replicates (each in technical triplicates), resulting in $n = 6$. Determined K_i values were compared using a t -test testing GraphPad Prism 8.2.1) for significantly different binding affinities comparing different formulations. n.s., not significant.

protruding into the CD cavity. Proton signal a, originating from the fluoro-substituted aromatic ring, is experiencing a similarly strong up-field shift (-0.06 ppm), even though the ring is not protruding into the cavity. However, it is in close vicinity to the carbonyl moiety of 4, which is forming HBs with the CD secondary face. According to the in silico simulations ligands 3 and 5 don't form HBs with OH-groups within the β -CD cavity. Consequently, observed NMR shifts originate from the deep intrusion of 3 and 5 into the CD cavity. Interestingly, ligands 3–5 behaved differently in silico regarding the positioning of their fluoro-substituted aromatic rings (Fig. 7). While the ring was protruding from the secondary face of ligand 3 and 4 ICs, it was protruding from the primary face regarding ligand 5. In contrast, the proton signals a (Fig. 5) determined during NMR experiments behaved very similar. In silico simulations resulted in several potential binding modes (data not shown) including different orientations of the fluoro-substituted aromatic ring of 3–5. Similar results were generated during in silico simulations regarding ligands 1 and 2, with two preferred binding modes for each of the respective ligands (data not shown). In silico results, suggesting more than one possible binding mode (or different ones at the same time) upon IC formation were further supported by 2D ^1H - ^1H NOESY NMR experiments (Fig. 6). Intermolecular correlations between

ligands 2–5 aromatic protons and H3 and H5 protons of 2-HP- β -CD clearly showed the co-existence of two different IC species (Fig. 6B–E) for each of those ligands. Moreover, the 2-HP- β -CD concentration-dependent deviation of ligands 3 and 5 from an AL-type behaviour indicative of a 1:1 IC stoichiometry (shown in Fig. 4B and D) suggest the possibility of higher-order host:guest stoichiometry (e.g. 1:2). The 2D NMR data of 3 and 5 (Fig. 6C and E) further support this hypothesis.

In summary, discrepancies between in silico and 2D NMR data could origin from the use of β -CD as a host molecule instead of 2-HP- β -CD during in silico simulations, but also the presence of 1:2 guest:host stoichiometries regarding the formation of ICs. At this point NMR data should be considered more valid. However, proper 2-HP- β -CD substitution patterns could allow for more detailed elaborations in future efforts [53–56].

While in silico simulations allow for highly valuable insights into potential complexation mechanisms considering ligand binding modes and HB formation, elucidation of IC stoichiometry further contributes to the detailed characterization of the different complexes (Fig. 4). Interestingly, IC stoichiometry didn't appear to impact D_2R -ligand binding behaviour in a systematic manner. Ligands 3, 4 and 5 showed different binding behaviours in vitro comparing their respective 'free' and IC

conditions (Fig. 9). However, **4** (Fig. 4C) showed a linear correlation during PSB studies, indicating a 1:1 stoichiometry. In contrast, **3** and **5** were characterized by a B_s-type curve (Fig. 1 and Fig. 4B and D) indicating only partially soluble ICs dependent on the 2-HP-β-CD concentration [58]. Ligand **2** also showed an A_L-type 1:1 behaviour (Fig. 4A) but no differences regarding its in vitro binding behaviour comparing 'free' and IC conditions (Fig. 11).

While CDs in general are described as GRAS compounds by the FDA, their potentially cell lytic characteristics due to their amphiphilic nature were also considered in this project (Fig. 8). In accordance with literature, 2-HP-β-CD started to exert cytotoxic effects only at high concentrations ≥ 5 mM [61]. While this threshold appears high, initially, solubility limits of investigated ligands have to be taken into consideration. Ligands **1** – **5** ICs were generated using 40 mM 2-HP-β-CD. However, during the in vitro experiments samples were diluted to a maximum concentration of 1 mM. This concentration didn't affect in vitro binding affinities (Fig. 10). However, test compounds with higher lipophilicity could be in need of higher 2-HP-β-CD concentrations to allow detailed investigations.

While cytotoxic events at 2-HP-β-CD concentrations ≤ 1 mM could be ruled out, concentrations ≥ 1 mM affected the specific signal read-out of the utilized cell-based in vitro HTRF assay (Fig. 9). Therefore, it was highly relevant to determine if ligand binding was affected using this concentration. Therefore, ligand **2** was used as a proof-of-concept to investigate this pitfall. K_i values between 'free' and different 2-HP-β-CD concentrations didn't differ significantly from each other (Fig. 11), thus validating the ligand specificity of the effects observed on **4** and **5**.

Ligands **1** and **3** behaved similar to **2**. While, in general, determined K_i values of **1** and **3** were higher (Table 5), in vitro binding behaviour was not affected upon the formation of ICs. Interestingly, **4** and **5** were characterized by significantly increased K_i values under IC conditions. Since all of them were investigated using 1 mM 2-HP-β-CD, based on the proof-of-concept results of **2** (Fig. 11), effects are suggested to be not cytotoxicity- but ligand structure-related. Again, this is also in accordance with the in silico results attributing the lowest overall binding energy to **4** and **5**. Thus, a stable IC could result in less free ligand leading to a decreased binding affinity in vitro. In contrast, well soluble ligands like **1** and **2**, even though ICs are generated in solution, can still exert their full receptor binding potential under IC conditions.

While the dose-dependent effect of ligand – 2-HP-β-CD was clearly highlighted within the presented work, future efforts should also include time-dependent binding affinity experiments. This is especially important, since the slow release of active compounds from ICs could further impact the binding behaviour/kinetics, thus, the in vitro characterization of novel compounds in drug discovery [62].

5. Conclusion

Investigating solubility under different conditions clearly showed the capability of 2-HP-β-CD to increase ligand concentrations in a structure-independent manner. Additionally, PSB studies allowed for an estimation of the 2-HP-β-CD concentration-dependent A_L-type behaviour, formation of higher order host:guest ICs as well as generation of insoluble complexes. NMR experiments confirmed the formation of the ICs and combined with in silico simulations enabled the elaboration of possible binding modes of the ligands within the β-CD cavity. Additionally, binding energies could be calculated while NMR chemical shift deviations allowed for the estimation of HB generation based on in silico simulations. While current literature considering low cytotoxicity of CDs could be supported employing a CTB cell viability assay, cell-based binding affinity studies showed the risk of impairing ligand binding affinity using 2-HP-β-CD. K_i values of ligands **1**–**3** remained unaffected by the formation of ICs. However, binding affinities of ligands **4** and **5** were impacted by the use of 2-HP-β-CD. Since the effects were significant (two- and three-fold reduction in binding affinity for **4** and **5**, respectively) those results should be included in current research efforts

with caution. While CDs actually appear to be GRAS compounds, our results show that they can affect target-binding affinity for specific compounds in vitro. We therefore recommend to carefully evaluate IC activity measurements in pharmacological characterisation of novel lipophilic research compounds, because IC formation may alter experimental results.

Funding

V.T. was funded by the Austrian Science Fund (FWF) project T942. L. Z. was funded by PMU-RIF, 2022-PRE-005-Zell. The computational results presented have been achieved (in part) using the HPC infrastructure LEO of the University of Innsbruck.

CRediT authorship contribution statement

Lukas Zell: Writing – review & editing, Writing – original draft, Visualization, Validation, Methodology, Investigation, Funding acquisition, Data curation, Conceptualization. **Thomas S. Hofer:** Writing – review & editing, Writing – original draft, Visualization, Validation, Methodology, Investigation, Data curation. **Mario Schubert:** Writing – review & editing, Writing – original draft, Visualization, Validation, Methodology, Investigation, Data curation. **Alexander Popoff:** Writing – review & editing, Validation, Methodology, Data curation. **Anna Höll:** Investigation, Data curation. **Moritz Marschhofer:** Investigation, Data curation. **Petra Huber-Cantonati:** Validation, Data curation. **Veronika Temml:** Writing – review & editing, Supervision, Project administration, Methodology, Funding acquisition, Conceptualization. **Daniela Schuster:** Writing – review & editing, Supervision, Resources, Project administration, Methodology, Funding acquisition, Conceptualization.

Declaration of competing interest

The authors declare that they have no known competing financial interests or personal relationships that could have appeared to influence the work reported in this paper.

Data availability

Data will be made available on request.

References

- [1] A. Cherkasov, et al., QSAR modeling: where have you been? Where are you going to? *J. Med. Chem.* 57 (12) (2014) 4977–5010, <https://doi.org/10.1021/jm4004285>.
- [2] C.A. Lipinski, Rule of five in 2015 and beyond: Target and ligand structural limitations, ligand chemistry structure and drug discovery project decisions, *Adv. Drug Deliv. Rev.* 101 (2016) 34–41, <https://doi.org/10.1016/j.addr.2016.04.029>.
- [3] C. Hansch, P. Maloney, T. Fujita, R. Muir, Correlation of biological activity of phenoxycetic acids with hammett substituent constants and partition coefficients, *Nature* 194 (1962) 178–180, <https://doi.org/10.1038/194178b0>.
- [4] S. Lobo, Is there enough focus on lipophilicity in drug discovery? *Expert Opin. Drug Discov.* 15 (3) (2020) 261–263, <https://doi.org/10.1080/17460441.2020.1691995>.
- [5] P.D. Leeson, S.A. St-Galley, The influence of the 'organizational factor' on compound quality in drug discovery, *Nat. Rev. Drug Discov.* 10 (10) (2011) 749–765, <https://doi.org/10.1038/nrd3552>.
- [6] P.D. Leeson, B. Springthorpe, The influence of drug-like concepts on decision-making in medicinal chemistry, *Nat. Rev. Drug Discov.* 6 (11) (2007) 881–890, <https://doi.org/10.1038/nrd2445>.
- [7] M.P. Gleeson, A. Hersey, D. Montanari, J. Overington, Probing the links between in vitro potency, ADMET and physicochemical parameters, *Nat. Rev. Drug Discov.* 10 (3) (2011) 197–208, <https://doi.org/10.1038/nrd3367>.
- [8] S. Basith, et al., Exploring G protein-coupled receptors (GPCRs) ligand space via Cheminformatics approaches: Impact on rational drug design, *Front. Pharmacol.* 9 (2018) 128, <https://doi.org/10.3389/fphar.2018.00128>.
- [9] R.M. Cooke, A.J. Brown, F.H. Marshall, J.S. Mason, Structures of G protein-coupled receptors reveal new opportunities for drug discovery, *Drug Discov. Today* 20 (11) (2015) 1355–1364, <https://doi.org/10.1016/j.drudis.2015.08.003>.
- [10] S. Azam, et al., G-protein-coupled receptors in CNS: A potential therapeutic target for intervention in neurodegenerative disorders and associated cognitive deficits, *Cells* 9 (2) (2020), <https://doi.org/10.3390/cells9020506>.

- [11] T.T. Wager, et al., Defining desirable central nervous system drug space through the alignment of molecular properties, in vitro ADME, and safety attributes, *ACS Chem. Neurosci.* 1 (6) (2010) 420–434, <https://doi.org/10.1021/cn100007x>.
- [12] A.K. Ghose, T. Herbertz, R.L. Hudkins, B.D. Dorsey, J.P. Mallamo, Knowledge-based, central nervous system (CNS) lead selection and lead optimization for CNS drug discovery, *ACS Chem. Neurosci.* 3 (1) (2012) 50–68, <https://doi.org/10.1021/cn200100h>.
- [13] E.A. Yasi, N.S. Kruyer, P. Peralta-Yahya, Advances in G protein-coupled receptor high-throughput screening, *Curr. Opin. Biotechnol.* 64 (2020) 210–217, <https://doi.org/10.1016/j.copbio.2020.06.004>.
- [14] C.A. Flanagan, GPCR-radioligand binding assays, *Methods Cell Biol.* 132 (2016) 191–215, <https://doi.org/10.1016/bs.mcb.2015.11.004>.
- [15] J.M. Zwier, et al., A fluorescent ligand-binding alternative using Tag-lite(R) technology, *J. Biomol. Screen.* 15 (10) (2010) 1248–1259, <https://doi.org/10.1177/1087057110384611>.
- [16] F. Degorce, et al., HTRF: A technology tailored for drug discovery - A review of theoretical aspects and recent applications, *Curr. Chem. Genomics* 3 (2009) 22–32, <https://doi.org/10.2174/1875397300903010022>.
- [17] M. Timm, L. Saaby, L. Moesby, E.W. Hansen, Considerations regarding use of solvents in in vitro cell based assays, *Cytotechnology* 65 (5) (2013) 887–894, <https://doi.org/10.1007/s10616-012-9530-6>.
- [18] C. Fink, et al., Evaluating the role of solubility in oral absorption of poorly water-soluble drugs using physiologically-based pharmacokinetic modeling, *Clin. Pharmacol. Ther.* 107 (3) (2020) 650–661, <https://doi.org/10.1002/cpt.1672>.
- [19] A. Sarabia-Vallejo, M.D.M. Caja, A.I. Olives, M.A. Martin, J.C. Menendez, Cyclodextrin inclusion complexes for improved drug bioavailability and activity: Synthetic and analytical aspects, *Pharmaceutics* 15 (9) (2023), <https://doi.org/10.3390/pharmaceutics15092345>.
- [20] F.B.T. Pessine, A. Calderini, G.L. Alexandrino, *Cyclodextrin Inclusion Complexes Probed by NMR Techniques, in Magnetic Resonance Spectroscopy*, D. Kim, Editor. 2012. p. 276. DOI: 10.5772/1228.
- [21] B.G. Poulson, et al., Cyclodextrins: Structural, chemical, and physical properties, and applications, *Polysaccharides* 3 (1) (2021) 1–31, <https://doi.org/10.3390/polysaccharides3010001>.
- [22] H. Dodziuk, *Molecules with Holes - Cyclodextrins*, in *Cyclodextrins and Their Complexes*, H. Dodziuk, Editor. 2006, John Wiley & Sons. DOI: 10.1002/3527608982.
- [23] S.W. Jun, et al., Preparation and characterization of simvastatin/hydroxypropyl-beta-cyclodextrin inclusion complex using supercritical antisolvent (SAS) process, *Eur. J. Pharm. Biopharm.* 66 (3) (2007) 413–421, <https://doi.org/10.1016/j.ejpb.2006.11.013>.
- [24] L. Szente, A. Singhal, A. Domokos, B. Song, Cyclodextrins: Assessing the impact of cavity size, occupancy, and substitutions on cytotoxicity and cholesterol homeostasis, *Molecules* 23 (5) (2018), <https://doi.org/10.3390/molecules23051228>.
- [25] A. Garcia, D. Leonardi, M.O. Salazar, M.C. Lamas, Modified beta-cyclodextrin inclusion complex to improve the physicochemical properties of albendazole. Complete in vitro evaluation and characterization, *PLoS One* 9 (2) (2014) e88234, <https://doi.org/10.1371/journal.pone.0088234>.
- [26] X. Hao, et al., Hydroxypropyl-beta-cyclodextrin-complexed resveratrol enhanced antitumor activity in a cervical cancer model: In vivo analysis, *Front. Pharmacol.* 12 (2021) 573909, <https://doi.org/10.3389/fphar.2021.573909>.
- [27] D. Duchene, A. Bocho, Thirty years with cyclodextrins, *Int. J. Pharm.* 514 (1) (2016) 58–72, <https://doi.org/10.1016/j.ijpharm.2016.07.030>.
- [28] A.S. Hauser, M.M. Attwood, M. Rask-Andersen, H.B. Schioth, D.E. Gloriam, Trends in GPCR drug discovery: New agents, targets and indications, *Nat. Rev. Drug Discov.* 16 (12) (2017) 829–842, <https://doi.org/10.1038/nrd.2017.178>.
- [29] F. Stocchi, M. Torti, C. Fossati, Advances in dopamine receptor agonists for the treatment of Parkinson's disease, *Expert Opin. Pharmacother.* 17 (14) (2016) 1889–1902, <https://doi.org/10.1080/14656566.2016.1219337>.
- [30] X. Pan, et al., Dopamine and dopamine receptors in Alzheimer's disease: A systematic review and network meta-analysis, *Front. Aging Neurosci.* 11 (2019) 175, <https://doi.org/10.3389/fnagi.2019.00175>.
- [31] J.C. Martel, S. Gatti McArthur, Dopamine receptor subtypes, physiology and pharmacology: New ligands and concepts in Schizophrenia, *Front. Pharmacol.* 11 (2020) 1003, <https://doi.org/10.3389/fphar.2020.01003>.
- [32] P. Li, G.L. Snyder, K.E. Vanover, Dopamine targeting drugs for the treatment of schizophrenia: Past, present and future, *Curr. Top. Med. Chem.* 16 (2019) 3385–3403, <https://doi.org/10.2174/1568026616666160608084834>.
- [33] S.A. Gegenschatz, F.A. Chiappini, C.M. Teglia, A. Munoz de la Pena, H. C. Goicoechea, Binding the gap between experiments, statistics, and method comparison: A tutorial for computing limits of detection and quantification in univariate calibration for complex samples, *Anal. Chim. Acta* 1209 (2022) 339342, <https://doi.org/10.1016/j.aca.2021.339342>.
- [34] T. Higuchi, K.A. Connors, Phase solubility techniques, *Adv. Anal. Chem. Instrum.* 4 (1965) 117–212, [https://doi.org/10.1016/S0076-6879\(82\)87029-8](https://doi.org/10.1016/S0076-6879(82)87029-8).
- [35] B.Y. Yang, J. Lin, Y. Chen, Binding behaviors of scutellarin with α -, β -, γ -cyclodextrins and their derivatives, *J. Incl. Phenom.* 64 (2009) 149–155, <https://doi.org/10.1007/s10847-009-9547-4>.
- [36] L. Tan, et al., Determination of apomorphine freebase in sublingual tablets by proton nuclear magnetic resonance spectroscopy, *J. Pharm. Biomed. Anal.* 129 (2016) 378–382, <https://doi.org/10.1016/j.jpba.2016.06.045>.
- [37] G.C. M'Bitsi-Ibouily, et al., Synthesis, characterisation and in vitro permeation, dissolution and cytotoxic evaluation of ruthenium(II)-liganded sulpiride and amino alcohol, *Sci. Rep.* 9 (1) (2019) 4146, <https://doi.org/10.1038/s41598-019-40538-1>.
- [38] C.A. Janicki, R.K. Gilpin, *Droperidol. Analytical Profiles of Drug Substances*, 1978. 7: p. 171-192. DOI: 10.1016/S0099-5428(08)60092-1.
- [39] C.A. Janicki, C.Y. Ko, *Haloperidol. Analytical Profiles of Drug Substances*, 1981. 9: p. 341-369. DOI: 10.1016/S0099-5428(08)60146-X.
- [40] C.E. Keller, W.R. Carper, NMR 1H relaxation and NOESY studies of spiperone conformational features in solution, *Magn. Reson. Chem.* 31 (1993) 566–572, <https://doi.org/10.1002/mrc.1260310609>.
- [41] H.E. Gottlieb, V. Kotlyar, A. Nudelman, NMR chemical shifts of common laboratory solvents as trace impurities, *J. Org. Chem.* 62 (21) (1997) 7512–7515, <https://doi.org/10.1021/jo971176v>.
- [42] D.J. Wales, J.P.K. Doye, Global optimization by basin-hopping and the lowest energy structures of Lennard-Jones clusters containing up to 110 atoms, *J. Phys. Chem.* 101 (28) (1997) 5111–5116, <https://doi.org/10.1021/jp970984n>.
- [43] C. Devereux, et al., Extending the applicability of the ANI deep learning molecular potential to sulfur and halogens, *J. Chem. Theory Comput.* 16 (7) (2020) 4192–4202, <https://doi.org/10.1021/acs.jctc.0c00121>.
- [44] M. Elstner, et al., Self-consistent-charge density-functional tight-binding method for simulations of complex materials properties, *Physica (1998)*, <https://doi.org/10.1103/PHYSREVB.58.7260>.
- [45] B. Hourahine, et al., DFTB+, a software package for efficient approximate density functional theory based atomistic simulations, *J. Chem. Phys.* 152 (12) (2020) 124101, <https://doi.org/10.1063/1.5143190>.
- [46] M. Gaus, A. Goez, M. Elstner, Parametrization and benchmark of DFTB3 for organic molecules, *J. Chem. Theory Comput.* 9 (1) (2013) 338–354, <https://doi.org/10.1021/ct300849w>.
- [47] M. Gaus, X. Lu, M. Elstner, Q. Cui, Parameterization of DFTB3/3OB for sulfur and phosphorus for chemical and biological applications, *J. Chem. Theory Comput.* 10 (4) (2014) 1518–1537, <https://doi.org/10.1021/ct401002w>.
- [48] M. Kubillus, T. Kubar, M. Gaus, J. Rezac, M. Elstner, Parameterization of the DFTB3 method for Br, Ca, Cl, F, I, K, and Na in organic and biological systems, *J. Chem. Theory Comput.* 11 (1) (2015) 332–342, <https://doi.org/10.1021/ct5009137>.
- [49] S. Grimme, S. Ehrlich, L. Goerigk, Effect of the damping function in dispersion corrected density functional theory, *J. Comput. Chem.* 32 (7) (2011) 1456–1465, <https://doi.org/10.1002/jcc.21759>.
- [50] A. Klamt, G. Schüürmann, COSMO: A new approach to dielectric screening in solvents with explicit expressions for the screening energy and its gradient, *J. Chem. Soc.* 5 (1993) 799–805, <https://doi.org/10.1039/P29930000799>.
- [51] W. Humphrey, A. Dalke, K. Schulten, VMD: Visual molecular dynamics, *J. Mol. Graph.* 14 (1) (1996), [https://doi.org/10.1016/0263-7855\(96\)00018-5](https://doi.org/10.1016/0263-7855(96)00018-5).
- [52] K. Kellett, D.R. Slochower, M. Schauerl, B.M. Duggan, M.K. Gilson, Experimental characterization of the association of beta-cyclodextrin and eight novel cyclodextrin derivatives with two guest compounds, *J. Comput. Aided Mol. Des.* 35 (1) (2021) 95–104, <https://doi.org/10.1007/s10822-020-00350-w>.
- [53] K. Kerdpol, et al., Cavity closure of 2-hydroxypropyl-beta-cyclodextrin: replica exchange molecular dynamics simulations, *Polymers (Basel)* 11 (1) (2019), <https://doi.org/10.3390/polym11010145>.
- [54] K. Hatzigiapiou, et al., Biophysical studies and in vitro effects of tumor cell lines of cannabidiol and its cyclodextrin inclusion complexes, *Pharmaceutics* 14 (4) (2022), <https://doi.org/10.3390/pharmaceutics14040706>.
- [55] E. Christoforides, A. Andreou, A. Papaioannou, K. Bethanis, Structural studies of piperine inclusion complexes in native and derivative beta-cyclodextrins, *Biomolecules* 12 (12) (2022), <https://doi.org/10.3390/biom12121762>.
- [56] C.W. Yong, C. Washington, W. Smith, Structural behaviour of 2-hydroxypropyl-beta-cyclodextrin in water: Molecular dynamics simulation studies, *Pharm. Res.* 25 (5) (2008) 1092–1099, <https://doi.org/10.1007/s11095-007-9506-y>.
- [57] L. Zell, C. Lainer, J. Kollar, V. Temml, D. Schuster, Identification of novel dopamine D(2) receptor ligands-A combined in silico/in vitro approach, *Molecules* (2022) 27 (14), <https://doi.org/10.3390/molecules27144435>.
- [58] P. Saokham, C. Muankaew, P. Jansook, T. Loftsson, Solubility of cyclodextrins and drug/cyclodextrin complexes, *Molecules* 23 (5) (2018), <https://doi.org/10.3390/molecules23051161>.
- [59] T. Loftsson, D. Hreinsdottir, M. Masson, Evaluation of cyclodextrin solubilization of drugs, *Int. J. Pharm.* 302 (1–2) (2005) 18–28, <https://doi.org/10.1016/j.ijpharm.2005.05.042>.
- [60] H. Günther, *NMR Spectroscopy: Basic Principles, Concepts, and Applications in Chemistry*. 3rd ed. 2013: Wiley-VCH.
- [61] M. Onishi, et al., Hydroxypropyl-beta-cyclodextrin spikes local inflammation that induces Th2 cell and T follicular helper cell responses to the coadministered antigen, *J. Immunol.* 194 (6) (2015) 2673–2682, <https://doi.org/10.4049/jimmunol.1402027>.
- [62] V.J. Stella, V.M. Rao, E.A. Zannou, V.V. Zia, Mechanisms of drug release from cyclodextrin complexes, *Adv. Drug Deliv. Rev.* 36 (1) (1999) 3–16, [https://doi.org/10.1016/s0169-409x\(98\)00052-0](https://doi.org/10.1016/s0169-409x(98)00052-0).